Hindawi
Advances in Civil Engineering
Volume 2019, Article ID 1487486, 11 pages
https://doi.org/10.1155/2019/1487486

Research Article

Artificial Seismic Source Field Research on the Impact of the Number and Layout of Stations on the Microseismic Location Error of Mines

Bao-xin Jia,[1,2] **Lin-li Zhou**,[1] **Yi-shan Pan**,[3] **and Hao Chen**[1]

[1]*School of Civil Engineering, Liaoning Technical University, Fuxin 123000, China*
[2]*Institute of Geology, China Earthquake Administration, Beijing 100000, China*
[3]*Liaoning University, Shenyang 110036, China*

Correspondence should be addressed to Bao-xin Jia; 13941855200@126.com

Received 2 September 2018; Accepted 6 December 2018; Published 22 January 2019

Academic Editor: Abdul Aziz bin Abdul Samad

A site experiment is performed herein within a 100 m range using a high-frequency structure activity monitor to explore the impact of different factors on the microseismic source location and analyze the range of influence of the velocity model, number of stations, and array surface on the seismic source location. Moreover, the impact of wave velocity, velocity-free location algorithm, and position of the seismic source on the microseismic location error of mines is discussed by establishing the ideal theoretical model of the wave velocity location and with particle swarm optimization. The impact of the number of stations and tables on the location precision is also explored by using the microseismic signals produced by the artificial seismic source. The results show that, for the location model containing the velocity, the velocity error would greatly affect the location precision, and the velocity-free algorithm receives good location results. The location result is more satisfactory when the seismic source point falls in between array envelope lines. The seismic source location precision is in direct proportion to the number of stations. According to the experiment, within a 100 m range, when the number of stations is over 12, the effect does not significantly grow with the increase of stations; the number of tables affects the location precision; and the multitable location effect is significantly superior to the single-table effect. The research shows that the optimal station density is 0.0192%, and the appropriate sensor layout to form a multitable monitoring network may effectively enhance the microseismic source precision of mines through the selection of a velocity-free location model. On the contrary, the number of stations can be reduced on the premise of the allowable error of the seismic source location, which may effectively reduce the monitoring cost.

1. Introduction

The shallow coal resource in China has already been exhausted in recent years; hence, the shift to deep coal mining is inevitable. The average mining depth of mines in China has already reached 700 m, and the number of deep shafts would increase year by year. However, a more complicated and dangerous stress environment would lead to more dynamic disasters in coal mines. Mine earthquake is one of these primary disasters, which usually give rise to a series of secondary disasters and result in a tremendous loss of personnel and property. Therefore, mine earthquake has become a challenge for both Chinese and foreign scholars and institutions [1, 2]. The microseismic monitoring system is widely applied in all coal mines [3–7]. To date, the microseismic monitoring technology has made great progress in research and application in the world, for example, in analyzing focal mechanisms [8], simulating three-dimensional (3D) geological structures [9, 10], estimating rock shear-wave velocity [11], and developing microseismic data processing software packages [12]. However, a prominent unresolved problem in the seismic monitoring is the large location error. Consequently, studies on improving the microseismic location precision would be of great theoretical significance and practical value.

Most of the current methods of microseismic location have been developed from earthquake locations. Accordingly, many scholars conducted studies on the location algorithm and how to improve the location precision. Several research directions on the decrease of the location error, such as the location algorithm [13], velocity model, station layout [14], and the accuracy of a seismic instrument [15, 16], have been presented. Thurber used the nonlinear Newton iteration method for location for the first time. Zhao and Zeng [17] then introduced the simplex method by relying on the rapid development of the computer. However, the simplex method has defects; for instance, it may easily fall in local error. Sabbione et al. [18] proposed an adaptive filtering method using the apex-shifted parabolic Radon transform to denoise downhole microseismic data. Dong [19] and Li et al. [20] proposed the velocity-free location method after considering the impact of the velocity error on the location precision. Afterward, Dong et al. [21] proposed the comprehensive location method based on a three-dimensional analysis of the acoustic emission and microseismic source in an unknown velocity system. Zhou et al. [22] proposed the microseismic source location method based on the small-region signal pickup. Increasing the number of stations is considered an effective method of improving the location precision; hence, Gong et al. [23] established the principle of determining the optimal number of channels by aiming at how to determine a proper number of stations. Gong et al. [24] believed that six channels could guarantee the location precision of the seismic source and proposed the anisotropic location method caused by the consideration of the anisotropic error. Lurka and Swanson [25] constructed a model according to the inversion principle and evolutionary algorithm for a deep coal mine in Western United States. This author then modified and improved the seismic location precision with a new target function model, and as a result, the seismic location precision was evidently enhanced compared with the constant velocity model. The station layout would affect the location precision. Kovaleva et al. [26] developed a comprehensive workflow to optimize the microseismic acquisition design and obtain optimum depth and location for deploying the borehole geophone arrays. Chen [27] studied the impact of a substation network on the location precision. After determining the optimal number of channels, Feng and Lan [28] conducted the optimal channel combiner fixed-point test to enhance the microseismic location precision. Jia and Li [29] proposed the reduction of the location error by optimizing the station layout. Ruigrok et al. [30] designed and applied a temporary array of 38 seismic stations. I. Sanina et al. [31] designed and applied a two-dimensional small-aperture seismic array. Meanwhile, Hu and Li [32] reduced the location error by accurately picking up the velocity of the P wave. Chen et al. [33] applied the ranking of the P wave to estimate the location error.

In conclusion, substantial research results have already been achieved for the microseismic source location. However, the abovementioned research mainly aims at the algorithm of a limited number of stations and station layout, and few comprehensive studies focused on the impact of comprehensive factors in a high-density station layout on the location error. In this study, an in situ microseismic monitoring experiment is conducted within a 100 m range for the first time with the high-frequency structure activity monitor to improve the microseismic location precision. Moreover, the impact of the location target function, velocity error, seismic source position, number of stations, and number of tables on the location precision is analyzed and studied by applying the theoretical analysis and field experimentation.

2. Microseismic Monitoring Experiment of an Artificial Seismic Source Site

Microseismic monitoring has become one of the effective methods of dynamic disaster control for all kinds of mines across the country, but location precision has always been a difficult problem to resolve. High-density station monitoring is considered an effective solution, but research on this topic is seldom performed in mines. Small-range microseismic monitoring is performed in this research. Moreover, a microseismic experiment site is built for the high-density station microseismic monitoring experiment, which can provide a theoretical basis for mine earthquake research.

2.1. Introduction to the Experimental Region. A gold mine in Fuxin was selected for the small-range microseismic monitoring experiment. The geographic coordinates of the mine are as follows: east longitude, 121°43′04″–121°43′06″, and north latitude, 41°53′03″–41°53′04″. The surface soil of the coal mine is mild clay, and rocks in the mine mainly include biotite plagioclase mylonite and felsic mylonite, which are solid and of good integrity. The mines are explored through vertical and inclined shafts in a single cage with a balanced weight. Coal mining currently has four midlevels, namely, mid-223 m, mid-180 m, mid-140 m, and mid-100 m. Among which, the first (mid-223 m) has already been emptied and abandoned. The top-down horizontal sublevel mining method is adopted according to the status of mine production and the hoisting condition of the ore body. Underground mining is being adopted at the present, and vertical shaft-blind inclined shaft is employed for codevelopment based on the full utilization of the original development system. A vertical shaft is employed for transportation from the surface to 180 m below the ground, while an inclined shaft is adopted from 180 m to 140 m and 180 m to 100 m plane. The experiment section is the plane of 140 m, 180 m, and 100 m.

2.2. Monitoring Instrument. Experiment monitoring includes sensors, cables, a 12-channel data hub, and a 48-channel data recorder for constructing the physical deformation site (Figure 1). The sensors used in the experiment adopt a direction-free setting. Sensors feature high sensitivity; hence, the data acquisition frequency can be set as 100,000 Hz at the maximum. While recording the microblasting signal in the experiment, the sampling frequency is set to 25 kHz.

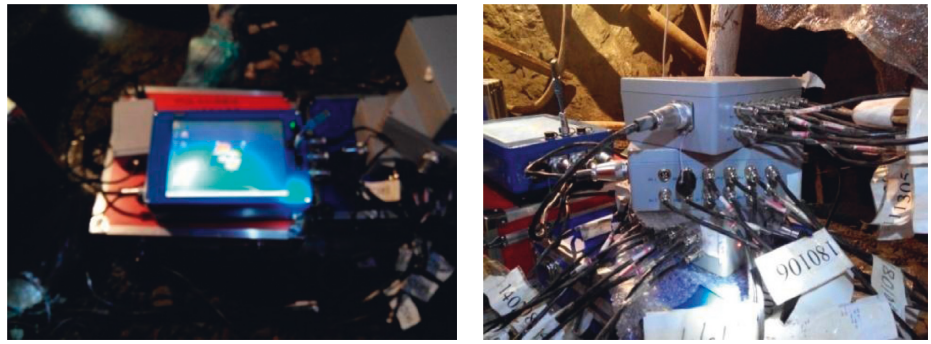

(a) (b)

Figure 1: Site monitoring equipment layout. (a) Data recorder. (b) Data hub.

2.3. Array Layout. Sensors were mainly laid out in three planes and two inclined shafts. The vertical size of the distribution region was 80 m, while the horizontal size was between 100 m and 200 m. The array mainly consisted of 33 sensors. Table 1 shows their location information. Figures 2–4 depict the planar layout of the sensor. Figure 5 shows the space layout of the sensors.

2.4. Microblasting Seismic Source. Three microblasting experiments were performed, and the blasting location was set in three operation planes. A monitoring station was set near the artificial seismic source to precisely collect the seismic moment. The arrival time difference of this station and the other monitoring stations was calculated and became the travel time of the seismic signal spent in reaching the detection station. Table 2 presents the artificial seismic source coordinates, amount of explosive, and the signal waveform recorded. Figure 5 illustrates the spatial arrangement of the artificial microseismic source.

The monitoring result showed that only the No. 2 blasting at the 140 m plane and the No. 3 blasting at the 100 m plane were well received. The No. 1 seismic signal at the 180 m plane and the effective acceptance amount of stations were quite dissatisfactory and thus abandoned. The analysis implied that this finding may be caused by the remote seismic location, the small amount of explosive, and the dense transportation channels, which affected the signal transmission from the artificial seismic source to all the sensors. Figure 6 shows the signal received by all stations after the second and third blasting. The picked up signals were filtered. Subsequently, onset time picking was then conducted, which was not elaborated here because of the length limit.

3. Seismic Source Location Algorithm

3.1. Modeling. Suppose the microseismic monitoring region is a cubic area of which the side length is 1000 m. The sensors are distributed at the eight vertexes, whose coordinates (unit: m) are A (0, 0, 0); B (1000, 0, 0); C (1000, 1000, 0); D (0, 1000, 0); E (0, 0, 1000); F (1000, 0, 1000); G (1000, 1000, 1000); and H (0, 1000, 1000). The equivalent velocity of the wave transmission in the medium in the theoretical model is simplified as $V = 5600$ m/s to make it convenient to explore the impact of different factors on the location error. The central point O of the monitoring region is (500, 500, 500). The location effect worked out for the seismic source within and without the region is studied. After the artificial seismic source coordinates and the velocity are given, the arrival time from the artificial seismic source to the sensors is worked out by supposing that the artificial seismic source is stirred at 0 moment and taken as the true value. The location calculation is then performed with the arrival time. The coordinates of seismic source points 1 to 11 are (500, 500, 500), (400, 400, 400), ... , (−500, −500, −500). Artificial seismic source points 1–6 are within the envelope line of the monitoring region (i.e., AG line), while points 7–11 are beyond the envelope line (i.e., extending line of AG). The arrival time from the artificial seismic source points to all sensors is 0.1 ms as the minimum unit in the round-off method to simulate the error caused by the onset time picking. Figure 7 shows the model.

3.2. Location Algorithm. Particle swarm optimization is an emerging evolutionary algorithm, which constantly collects the direction and speed of search according to the flight course and information transfer between swamps. The search process is mainly accomplished by relying on the interactions and the mutual influence of particles featuring easy implementation, fast convergence, and high precision. The free flight of "particle swarm" in the solution space can perfectly resolve the problem of the final solution being the local optimal solution. The updated versions of the speed and the location of particle i are shown in the following equations:

$$\begin{aligned} V_{id} &= wV_{id} + c_1 r_1 \left(P_{id} - X_{id}\right) + c_2 r_2 \left(P_{gd} - X_{id}\right), \\ X_{id} &= X_{id} + V_{id}, \end{aligned} \tag{1}$$

where w is the inertia weight; c_1 and c_2 are the integrals ranging between [2, 4] known as the learning or accelerated factor; r_1 and r_2 are the random numbers between [0, 1] known as the maximum inertia weight and minimum inertia weight, respectively; $d = 1, 2, 3, \ldots, D$, where D stands for

Table 1: Sensor location information.

Plane	Number	Data hub and interface serial number	Sensor number	Coordinates (m)		
				X	Y	Z
180 m plane	6	1	3	180103	8835.730	6146.960	180.816
			4	180104	8832.982	6121.473	180.760
			5	180105	8851.786	6124.607	180.740
			6	180106	8854.521	6108.712	180.675
			7	180107	8879.863	6114.670	180.968
			8	180108	8834.896	6103.363	180.469
Short inclined shaft	3	1	9	110101	8883.636	6197.365	150.355
			10	110102	8878.167	6185.213	156.285
			11	110103	8867.835	6160.976	169.305
140 m plane	12	2	1	140201	8860.325	6241.630	141.353
			2	140202	8879.256	6235.671	139.650
			3	140203	8902.053	6225.357	139.590
			4	140204	8924.206	6221.107	139.550
			5	140205	8924.527	6201.975	139.608
			6	140206	8918.945	6182.133	139.723
			7	140207	8908.220	6174.085	139.716
			8	140208	8919.876	6314.837	139.925
			9	140209	8927.746	6244.410	139.580
			10	140210	8932.245	6261.876	139.619
			11	140211	8932.629	6279.137	139.628
			12	140212	8922.516	6308.026	139.820
100 m plane	6	3	1	100301	8851.300	6321.265	100.070
			2	100302	8858.368	6321.290	101.796
			3	100303	8868.516	6315.367	100.398
			4	100304	8882.840	6324.850	101.010
			5	100305	8925.043	6335.871	100.521
			6	100306	8894.740	6323.830	100.150
Long inclined shaft	6	3	7	111301	8838.087	6170.980	171.156
			8	111302	8840.036	6193.240	160.305
			9	111303	8841.736	6212.716	150.793
			10	111304	8845.730	6264.803	125.880
			11	111305	8847.221	6284.368	115.830
			12	111306	8848.507	6308.935	103.820

the dimension of the solution vector; V_{id}, X_{id}, P_{id}, and P_{gd} are the flight speed of particle i in the dth dimension space, location, optimal solution searched, and optimal solution searched by the swamp.

The location was worked out through the MATLAB PSO toolbox with the following PSO parameter settings: learning factor: $c_1 = c_2 = 2$; inertia weight: $r_1 = 0.9$, $r_2 = 0.4$; number of particles: 20, $w = 1$; and end condition: maximum number of iterations = 20,000 or $\varepsilon = 1e - 25$. When the velocity is known, $V = 5600$ m/s and $D = 3$. Meanwhile, $D = 4$ when the location is worked out with the unknown velocity.

3.2.1. Impacts of the Location Methods on the Location. This study located the two target functions of the known wave velocity and the unknown wave velocity through the ion swarm algorithm to explore the effects of different location methods on the location error. Equation (2) is the target function for solving the known wave velocity localization, and equation (3) is the target function for solving the unknown wave velocity localization; Figure 8 shows the location result error:

$$f = \min \sum_{i=1}^{n} \left(\Delta \hat{t}_{ij} - \Delta t_{ij}\right)^2 = \min \sum_{i=1}^{n} \left(t_i - t_j - \frac{l_i - l_j}{v}\right)^2, \tag{2}$$

$$f = \min \left\| \left(t_i - t_j\right)v - \left(l_i - l_j\right) \right\|. \tag{3}$$

Figure 8(a) illustrates that with the known wave velocity, the errors in the x, y, and z directions tended to increase with the source point away from the center of the monitoring station envelope. The error presented a jump change when the unknown wave velocity was used for the location, with the location error of each source point getting farther and farther away from the center point of the monitoring station. The location error was smaller in the area. The error outside the area also increased when the distance increased and became greater than the location error of the known wave velocity. Figure 8(b) depicts a large difference of the location error between

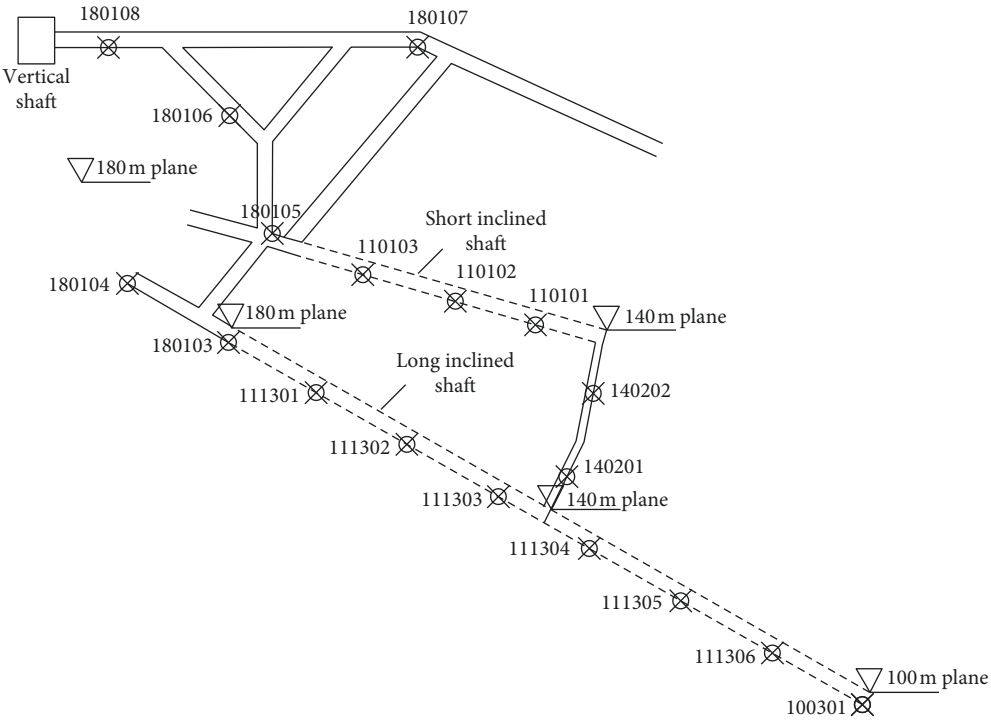

Figure 2: 180 m plane and inclined shaft sensor layout.

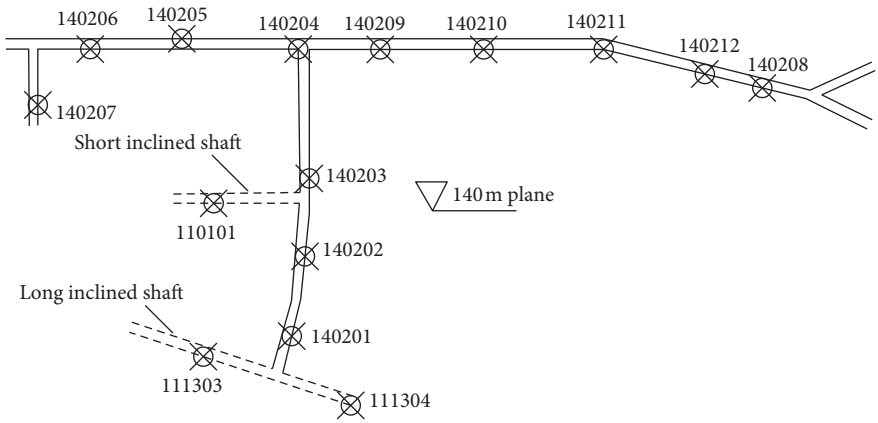

Figure 3: 140 m plane sensor layout.

the known and unknown wave velocities, which cannot reflect the actual geologic wave velocity. The influences of the two location methods on the location error were not obvious when the wave velocity error was not considered. However, the variation trend of the location error was different.

3.2.2. Influences of the Wave Velocity Error on the Location. The P-wave velocity of the rock samples in the experimental area was first required to be determined by an ultrasonic velocity meter based on the known wave velocity model for the location. Differences between the given wave velocity and the actual wave velocity were observed. Therefore, the errors that are ±2%, ±5%, ±10%, and ±15% are applied to disturb the original wave velocity V = 5600 m/s and take it as the true value of wave velocity. A disturbance error greater than 0 implied that the actual wave velocity was less than V; otherwise, the actual wave velocity was greater than V. The arrival time was calculated and taken as the initial value of the location calculation together with V = 5600 m/s to verify the influences of the wave velocity error on the location. Figure 9 shows the location distance error of each artificial seismic source under different wave velocity error disturbances.

Figure 9 also depicts that the wave velocity error has a great influence on the location performance when the known wave velocity was used for the location. The location error of each source point increased in line with the increase of the wave velocity error when the actual wave velocity was less than that used for the location. Meanwhile, the location error of

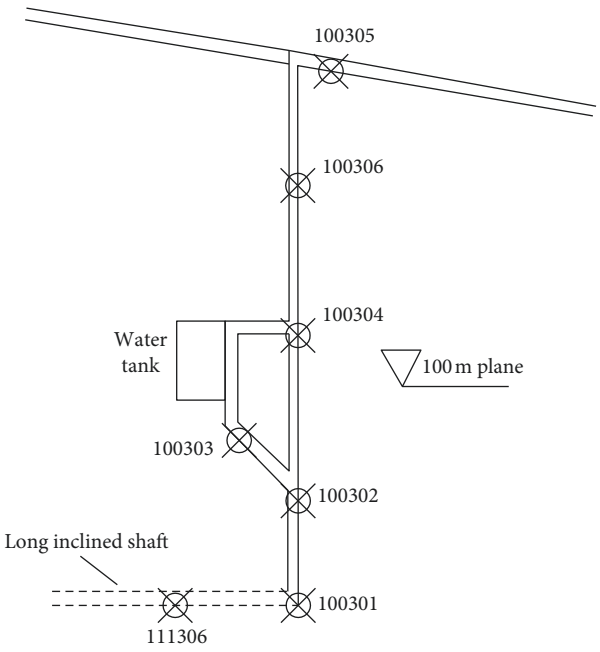

Figure 4: 100 m plane sensor layout.

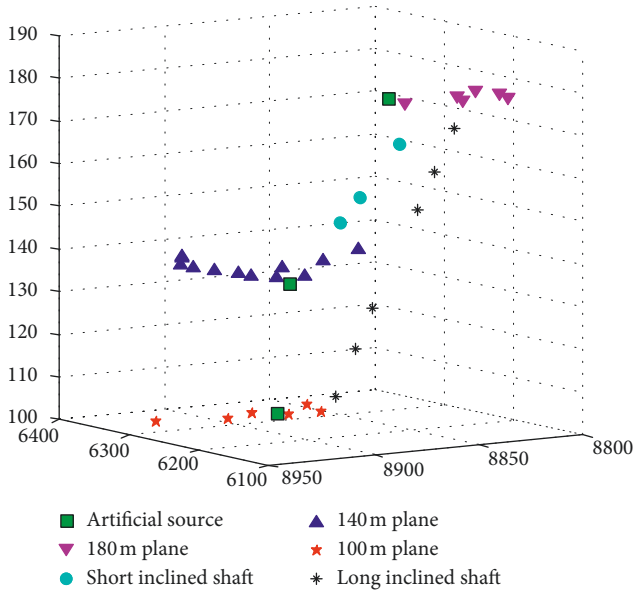

Figure 5: Sensor and artificial source space layout.

each source point inside the area increased in line with the increase of the wave velocity error when the actual wave velocity was greater than that used for the location. The location error of each source point outside the area was greater than that inside the area that approximately showed an exponential increase with the increase of the wave velocity error. The error brought by a lower location wave velocity was generally larger with a greater influence on the location.

3.2.3. Influences of the Source Position on the Location. Figure 10 clearly shows that the location error of each source point inside and outside the monitoring area was significantly different. The location error increased in a straight line with the enlarged distance from the central point inside the area when the actual wave velocity was greater than location wave velocity, and the disturbed value was less than −5%. The change rate of the error suddenly became higher from source point 6 (i.e., the demarcation point between the inside and the outside) and then became lower. Its position of becoming smaller became farther and farther away with the decrease of the disturbed value. In addition, the change rate of the error eventually tended to be stable. The disturbed value was greater than 5% when the actual wave velocity was less than the location wave velocity. The location error first increased and then decreased with the enlarged distance from the central point inside the area and gradually increased again with a more enlarged distance from the demarcation point. The location error was very small when the disturbed value was ±2%. This error slowly increased in a straight line inside the area, but remained stable outside the area. The influences of the source position on the location are suggested to be interfered by the wave velocity error. With the great error in the wave velocity, the location error changes could be divided into the three following areas from the central point of the area (Figure 10): near enlarged, mutation, and far enlarged areas. The change trend of the location error changed within the mutation area. Furthermore, the range and the changing characteristics of the mutation area depended on the wave velocity error.

4. Analysis on the Influences of the Quantity of Station Planes and Stations on the Location Error

The particle swarm algorithm was applied to undertake the source location to the microexplosion performed on the site. The location parameters are as follows: location area coordinates X = [8800, 9000], Y = [6100, 6400], and Z = [95, 185]. The effective arrival time was adopted for the location. The ultrasonic testing indoor showed that the P-wave velocity of the rock samples of the experimental diggings was 6357 m/s. The unknown wave velocity was adopted for the microexplosion source location to avoid the influences of the wave velocity error on the location performance.

4.1. Influences of the Quantity of Station Planes on the Location. Different station sensors, including 180 m plane, 140 m plane, 100 m plane, inclined shaft (long and short inclined shafts), and some plane sensors, were successively applied for the location to analyze the high-density array for the location performance of microseismic monitoring. The unknown wave velocity location was adopted for a better location performance (Figure 11). When the single station plane was used for the location, the source location was more accurately realized only when the source was located on or nearby the monitoring plane. The single location of the monitoring plane far away from the source would have an extremely great error, especially the vertical location error. When the sensor of the 140 m plane was adopted for the location of the 100 m plane, its vertical error unexpectedly

Table 2: Microblasting source.

Seismic source no.	Location	Number	Explosive amount	Coordinates (m)			Example of the signal waveform
				X	Y	Z	
1	180 m plane	1	300 g	8882.635	6127.475	181.028	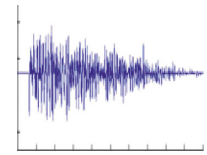
2	140 m plane	1	300 g	8917.753	6171.168	139.620	
3	100 m plane	1	400 g	8870.609	6316.663	100.096	

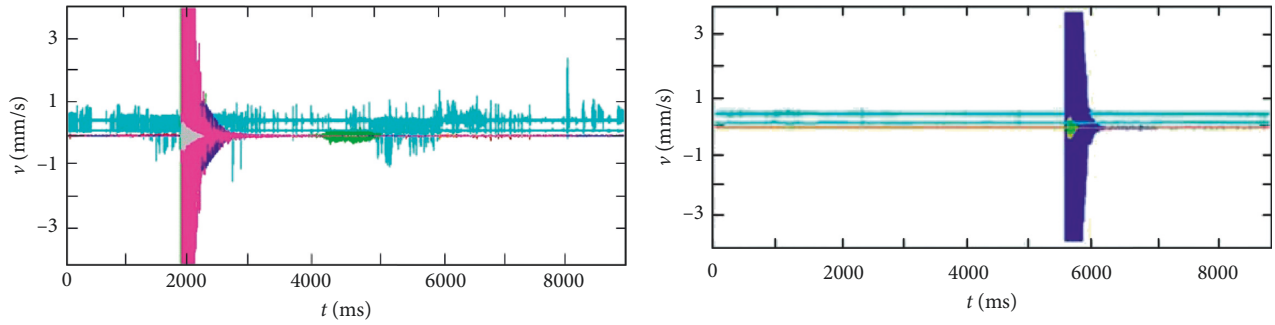

Figure 6: Microblasting signal. (a) No. 2 seismic source signal at the 100 m plane. (b) No. 3 seismic signal at the 140 m plane.

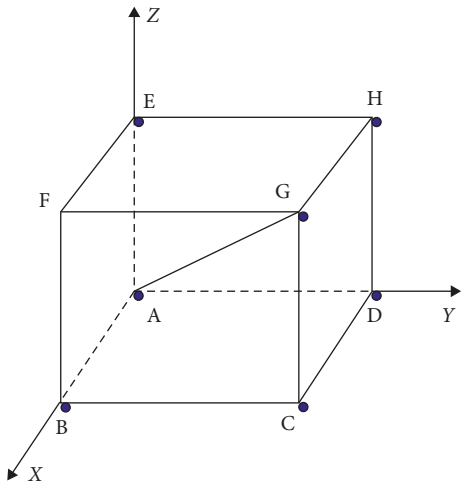

Figure 7: Model of the monitoring region.

reached 51 m, and the vertical distance between the two planes was only 40 m. The location performance was obviously greater than that of the single plane when two monitoring planes were applied for the location. However, this value was still less than that in the location with all the sensors used. This finding illustrates that the increase of the sensor "array plane" could largely reduce the location error with a positive and stimulating influence on the microseismic location.

4.2. Influences of the Station Quantity on the Location. Four sensors were selected from all the sensors in the array to verify the impact of the monitoring array density on the location performance and avoid locating in a single plane. The sensors at the other positions were successively superimposed to select different sensor quantities and perform an unknown wave velocity location for the microblasting on the 140 m plane. Three sets of data were selected to take the mean value for the location. Figure 12 shows the resulting location error. The left figure depicts that the sensor quantity plays a positive role in improving the location accuracy of the source. The location errors became increasingly smaller as the sensor quantity increased. The derivation was taken for the location error to obtain the variation trend curve of the error. As shown in the right side of Figure 12, the location error decreased with the increase of the sensor quantity when the sensor quantity was between 4 and 14. The value change of the derivative then became slow but was still less than 0, thereby indicating that the increase of the sensor quantity can improve the location performance, which proves that the high-density array is beneficial to control the microseismic monitoring accuracy. The source location error of the whole array was approximately 2.6 m. The mathematical relationship between the location error ΔL and the sensor quantity n was obtained as shown in equation (4) based on the fitting of the location error data in the figure. The correction determination coefficient Adj. R^2 = 0.98972, which shows that the fitting result is very close to the real situation. Through this equation, an exponential relationship can be found between both:

$$\overline{\Delta L} = 251.999 \times e^{-(n/2.343)} + 3.166. \quad (4)$$

In the above calculation, the P-wave velocities of the 140 m plane and the 100 m plane obtained from the

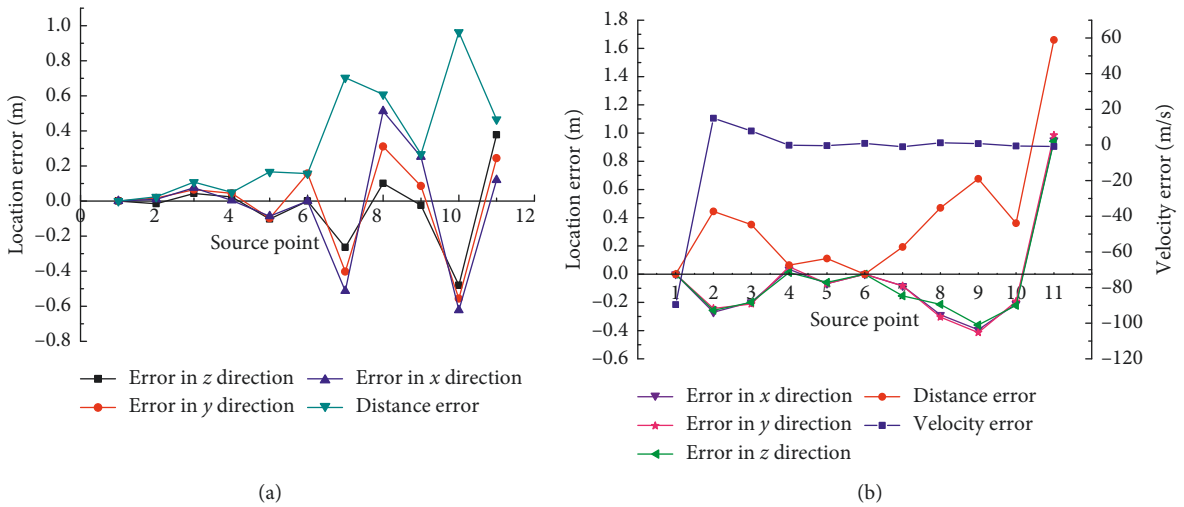

Figure 8: (a) Location error distribution under the known wave velocity. (b) Location error distribution under the unknown wave velocity.

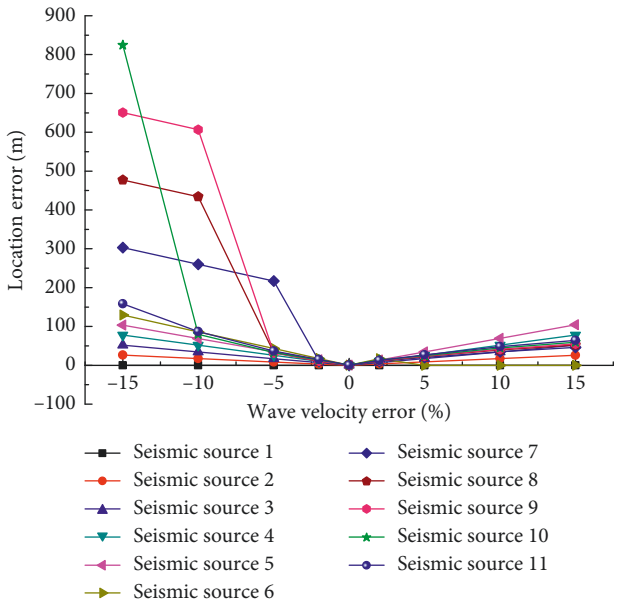

Figure 9: Location distance error distribution of different wave velocity errors.

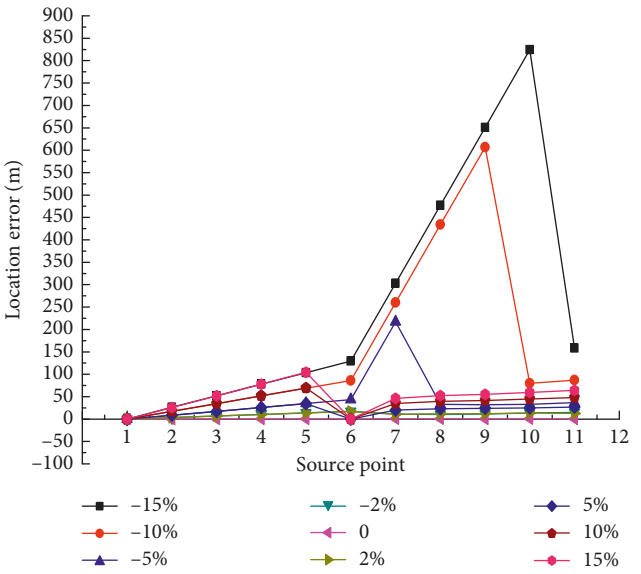

Figure 10: Location distance error distribution of different positions.

inversion of the whole array were 5898 m/s and 5903 m/s, respectively, which were rather different from the results of the indoor experiment. In addition, compared with the model analysis results, the location error of the actual monitoring was larger and related to the complexity of a geological structure. The location, size, and direction of various discontinuity surfaces, such as fractures, joints, and faults in the rock mass, all influence the wave propagation in the medium. Inevitably, errors were found in the arrival time required for the location because the time was acquired from the waveform recorded in the noise environment through phase identification. On the one hand, the high-density array microseismic monitoring can extend the quantity of the arrival time data to reduce the significant impact of the arrival time error. On the other hand, the high-density station, especially when being three-dimensionally laid, decreases the travel time distance from the source to the various sensors and reduces the difference between space and time and the theoretical calculation of the travel time data caused by the inhomogeneity of the rock mass. In summary, benefitting from the two abovementioned points, the high-density station can effectively improve the location performance of the microseismic source of the mine.

5. Conclusions

The following conclusions are obtained from this study:

(1) Theoretical modeling was used herein to analyze the target function with the wave velocity, nonwave velocity, and source location performance. Consequently, the wave velocity error had a great influence

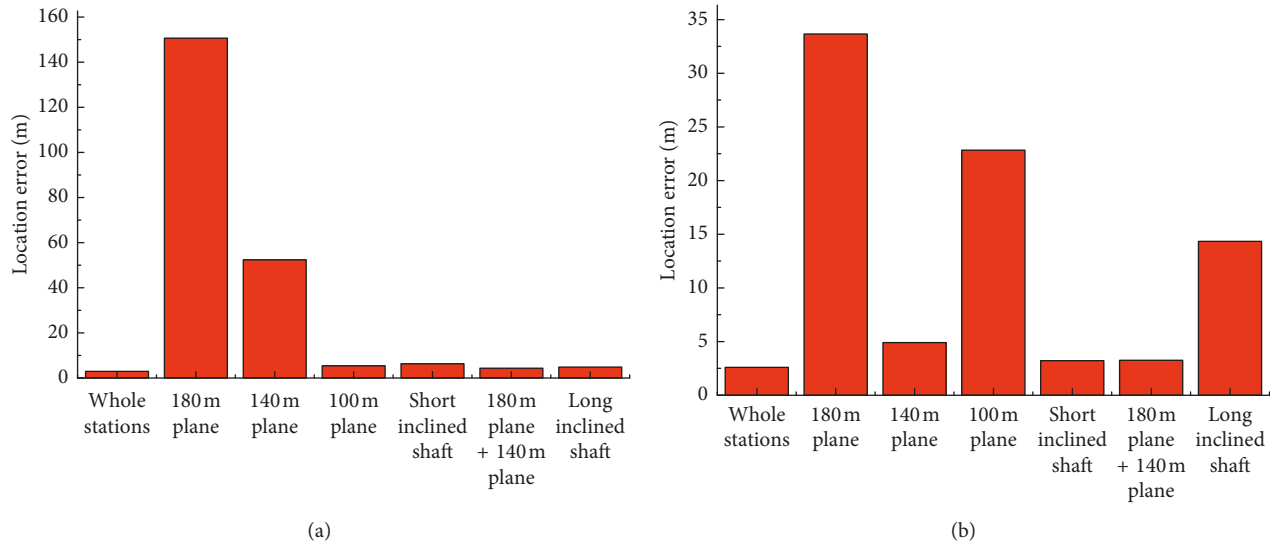

FIGURE 11: Relationship between the location error and the sensor position. (a) 100 m plane seismic source location error. (b) 140 m plane seismic source location error.

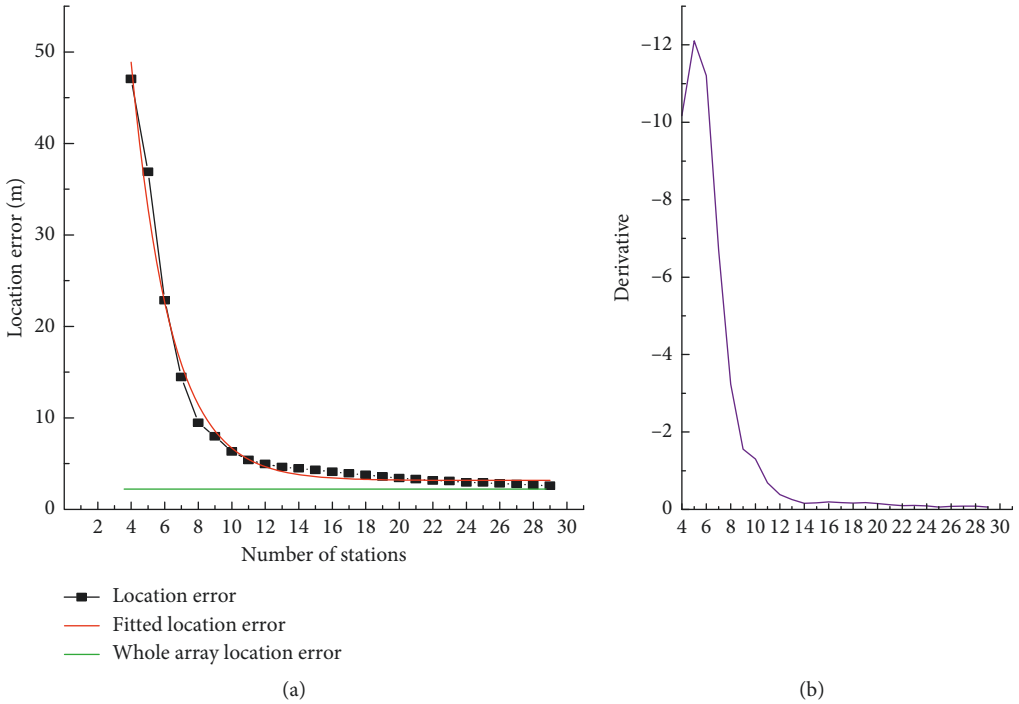

FIGURE 12: Relationship between the location error and the number of stations.

on the location result in the target function with the wave velocity, and such influence exponentially increased. The positioning error was small when the source point was at the envelope center of the monitoring array. The error was larger when the source point was outside the envelope.

(2) The influence of the station density on the location error was analyzed by a field experiment. The experimental results indicated that the influence of the station density can be divided into two parts: station quantity and station plane quantity. The location accuracy significantly increased with the increase of the station quantity when the station plane quantity was certain. When station quantity was more than 12, such an increase was no longer obvious. When the station quantity is certain, the increase of the station plane quantity can significantly improve the location accuracy. The accuracy of the multistation plane was higher than that of the single-station plane. The best station density was 0.0192%.

Data Availability

The data used to support the findings of this study are available from the corresponding author upon request.

Conflicts of Interest

The authors declare that there are no conflicts of interest regarding the publication of this paper.

Acknowledgments

The authors would like to express their gratitude to all those who helped them during the writing of this thesis. First of all, the author is grateful for the site and technical support of the manager and technical staff of the Fuxin Xinmin gold mine. Second, the authors are thankful to the postgraduates of Liaoning Technical University for their help in the experiments. Lastly, the authors would like to thank Editage (http://www.editage.cn) for the English language editing. This work was supported by the National Natural Science Foundation of China, grant no. 51774173; the Natural Science Foundation of Liaoning Province, China, grant no. 201602351; and the Open Fund for the State Key Laboratory of Seismological Dynamics, grant no. LED2015B01.

References

[1] S. J. Gibowicz and A. Kijko, *An Introduction to Mining Seismology*, Academic Press Inc, New York, NY, USA, 1994.

[2] Y. M. Yin, F. X. Jiang, G. X. Xie et al., "Relation between coal-rock failure and methane emission based on microseismic and dynamic stress monitoring," *Journal of Mining and Safety Engineering*, vol. 32, no. 2, pp. 325–330, 2015.

[3] A.-y. Cao, L.-m. Dou, G.-x. Chen, S.-y. Gong, Y.-g. Wang, and Z.-h. Li, "Focal mechanism caused by fracture or burst of a coal pillar," *Journal of China University of Mining and Technology*, vol. 18, no. 2, pp. 153–158, 2008.

[4] Y. S. Pan, Y. F. Zhao, F. H. Guan et al., "Study on rockburst monitoring and orientation system and its application," *Chinese Journal of Rock Mechanics and Engineering*, vol. 26, no. 5, pp. 1002–1011, 2007.

[5] L. M. Dou, J. He, S. Y. Gong et al., "A case study of micro-seismic monitoring: goaf water-inrush dynamic hazards," *Journal of China University of Mining and Technology*, vol. 41, no. 1, pp. 20–25, 2012.

[6] X. F. Xu, L. M. Dou, A. Y. Cao et al., "Effect of overlying strata structures on rock burst and micro-seismic monitoring analysis," *Journal of Mining and Safety Engineering*, vol. 28, no. 1, pp. 11–15, 2011.

[7] S. Y. Gong, L. M. Dou, A. Y. Cao et al., "Study on optimal configuration of seismological observation network for coal mine," *Chinese Journal of Geophysics*, vol. 53, no. 2, pp. 457–465, 2010.

[8] L. Fojtíková, V. Vavryčuk, A. Cipciar, and J. Madarás, "Focal mechanisms of micro-earthquakes in the dobrá voda seismoactive area in the malé karpaty mts. (little carpathians), Slovakia," *Tectonophysics*, vol. 492, no. 1–4, pp. 213–229, 2010.

[9] J. Rhie and D. Dreger, "A simple method for simulating microseismic H/V spectral ratio in 3D structure," *Geosciences Journal*, vol. 13, no. 4, pp. 401–406, 2010.

[10] K. B. Danilov and B. Konstantin, "The structure of the onega downthrown block and adjacent geological objects according to the microseismic sounding method," *Pure and Applied Geophysics*, vol. 174, no. 7, pp. 2663–2676, 2017.

[11] A. V. Gorbatikov, A. V. Kalinina, V. A. Volkov, J. Arnoso, R. Vieira, and E. Velez, "Results of analysis of the data of microseismic survey at lanzarote island, canary, Spain," *Pure and Applied Geophysics*, vol. 161, no. 7, pp. 1561–1578, 2004.

[12] D. V. Popov, K. B. Danilov, R. A. Zhostkov, Z. I. Dudarov, and E. V. Ivanova, "Processing the digital microseismic recordings using the data analysis kit (DAK) software package," *Seismic Instruments*, vol. 50, no. 1, pp. 75–83, 2014.

[13] A. Auger and N. Hansen, "Performance evaluation of an advanced local search evolutionary algorithm," in *Proceedings of the 2005 IEEE Congress on Evolutionary Computation*, no. 2, pp. 1777–17842, Edinburgh, Scotland, September 2005.

[14] Y. Sato and D. Skoko, "Optimum distribution of seismic observationpoints III," *Bulletin of the Earthquake Research Institute University of Tokyo*, vol. 43, no. 1, pp. 451–457, 1965.

[15] A. T. Ringler, T. Storm, L. S. Gee, C. R. Hutt, and D. Wilson, "Uncertainty estimates in broadband seismometer sensitivities using microseismics," *Journal of Seismology*, vol. 19, no. 2, pp. 317–327, 2014.

[16] A. T. Ringler, R. Sleeman, C. R. Hutt et al., *Seismometer Self-Noise and Measuring Methods*, Springer, Berlin, Heidelberg, 2015.

[17] Z. Zhao and R. S. Zeng, "A method for improving the determination of earthquake hypocenters," *Chinese Journal of Geophysics*, vol. 30, no. 4, pp. 379–388, 1987.

[18] J. I. Sabbione, M. D. Sacchi, and D. R. Velis, "Radon transform-based microseismic event detection and signal-to-noise ratio enhancement," *Journal of Applied Geophysics*, vol. 113, pp. 51–63, 2015.

[19] L. J. Dong, "Mathematical functions and parameters for microseismic source location without pre-measuring speed," *Chinese Journal of Rock Mechanics and Engineering*, vol. 30, no. 10, pp. 2057–2067, 2011.

[20] J. Li, Y. T. Gao, Y. L. Xie et al., "Improvement of microseismic locating based on simplex method without velocity measuring," *Chinese Journal of Rock Mechanics and Engineering*, vol. 33, no. 7, pp. 1336–1346, 2014.

[21] L. J. Dong, X. B. Li, J. Ma et al., "Three-dimensional analytical comprehensive solutions for acoustic emission/microseismic sources of unknown velocity system," *Chinese Journal of Rock Mechanics and Engineering*, vol. 36, no. 1, pp. 186–197, 2017.

[22] M. B. Zhou, J. X. Wu, and W. Zhang, "Microseismic source location method based on small area signal pickup," *Safety and Environmental Engineering*, vol. 22, no. 5, pp. 154–157, 2015, in Chinese.

[23] S. Y. Gong, L. M. Dou, X. P. Ma et al., "The method to identify the optimal channel numbers for increasing the location accuracy of microseismic events in coal mine," *Journal of China Coal Society*, vol. 35, no. 12, pp. 2017–2021, 2012.

[24] S. Y. Gong, L. M. Dou, X. P. Ma et al., "Study on the construction and solution technique of anisotropic velocity model in the location of coal mine tremor," *Chinese Journal of Geophysics-Chinese Edition*, vol. 55, no. 5, pp. 1757–1763, 2012.

[25] A. Lurka and P. Swanson, "Improvements in seismic event locations in a deep western U.S. coal mine using tomographic velocity models and an evolutionary search algorithm," *Mining Science and Technology (China)*, vol. 19, no. 5, pp. 599–603, 2009.

[26] Y. Kovaleva, M. Ostadhassan, N. Tamimi, and A. Kovalev, "A preliminary optimization of borehole microseismic array design with a multiple criteria decision analysis," *Journal of Applied Geophysics*, vol. 157, pp. 87–95, 2018.

[27] F. B. Chen, "Influence of distribution of mine microseismic locating subnet on positioning accuracy," *Coal Mining Technology*, vol. 21, no. 4, pp. 107–114, 2016, in Chinese.

[28] M. H. Feng and H. Lan, "Optimal channel combination fixed point test research for improving micro-seismic positioning accuracy of coal mine," *China Coal*, vol. 10, pp. 38–41, 2016, in Chinese.

[29] B. X. Jia and G. Z. Li, "The research and application for spatial distribution of mines seismic monitoring stations," *Journal of China Coal Society*, vol. 35, no. 12, pp. 2045–2048, 2010.

[30] E. Ruigrok, D. Draganov, M. Gómez et al., "Malargüe seismic array: design and deployment of the temporary array," *European Physical Journal Plus*, vol. 127, no. 10, p. 126, 2012.

[31] I. A. Sanina, S. G. Volosov, O. A. Chernykh, V. E. Asming, A. M. Soldatenkov, and O. Y. Riznichenko, "The design and experimental use of the Mikhnevo 2D small aperture seismic array," *Seismic Instruments*, vol. 44, no. 1, pp. 1–11, 2008.

[32] J. Y. Hu and S. L. Li, "Optimization of picking mine microseismic P-wave arrival time and its application in reducing error of source locating," *Machine Building and Automation*, vol. 36, no. 10, pp. 1940–1946, 2014.

[33] F. B. Chen, J. L. Liu, and Y. J. Wang, "Location error estimation of mine micro-seismic epicenter based on sequencing of P-wave arrival time," *Mining Safety and Environmental Protection*, vol. 43, no. 6, pp. 58–62, 2016.